Hyperspectral measurements of yellow rust and fusarium head blight in cereal crops: Part 1: Laboratory study

Rebecca L Whetton[a], Kirsty L Hassall[b], Toby W Waine[a], and Abdul M Mouazen[c]*

[a]Cranfield Soil and AgriFood Institute, Cranfield University, Bedfordshire MK43 0AL, UK.

[b]Department of Computational and Analytical Sciences, Rothamsted research, Harpenden, Hertfordshire AL5 2JQ

[c]Department of Soil Management, Ghent University, Coupure 653, 9000 Gent, Belgium.

E-mail of corresponding author: Abdul.Mouazen@UGent.be

Abstract

This paper assesses the potential use of a hyperspectral camera for measurement of yellow rust and fusarium head blight in wheat and barley canopy under laboratory conditions. Scanning of crop canopy in trays occurred between anthesis growth stage 60, and hard dough growth stage 87. Visual assessment was made at four levels, namely, at the head, at the flag leaves, at 2nd and 3rd leaves, and at the lower canopy. Partial least squares regression (PLSR) analyses were implemented separately on data captured at four growing stages to establish separate calibration models to predict the percentage coverage of yellow rust and fusarium head blight infection. Results showed that the standard deviation between 500 and 650 nm and the squared difference between 650 and 700 nm wavelengths were found to be significantly different between healthy and infected canopy particularly for yellow rust in both crops, whereas the effect of water-stress was generally found to be unimportant. The PLSR yellow rust models were of good prediction capability for 6 out of 8 growing stages, a very good prediction at early milk stage in wheat and a moderate prediction at the late milk development stage in barley. For fusarium, predictions were very good for seven growing stages and of good performance for anthesis growing stage in wheat, with best performing for the milk development stages. However, the root mean square error of predictions for yellow rust were almost half of those for fusarium, suggesting higher prediction accuracies for yellow rust measurement under laboratory conditions.

Key words

Yellow rust (*Puccinia striiformis*), fusarium head blight (*Fusarium graminearum*), wheat, barley, crop canopy, partial least squares regression.

1 Introduction

With the world's population estimated to reach 9 billion by 2050, sustainable approaches to increase crop yield are a necessity (Hole *et al.,* 2005; Godfray *et al.,* 2010). Current farming practices are unsustainable, relying on external inputs and high-yield varieties susceptible to disease (Hole *et al.,* 2005). Site specific management of inputs would reduce the amount required (Wittery and Mallarino 2004; Maleki *et al.,* 2007). Among these resources, fungicide application may well be reduced by targeted site specific spraying (FRAC 2010). However, accurate measurement of fungal diseases is a main requirement for sustainable application of fungicides, and expected to contribute to the reduction and prevention of the spread of crop disease and the losses of quantity and quality incurred from them.

Fungal disease control is a large task for a successful production of cereals worldwide. Both yellow rust and fusarium are fungal diseases which infect small cereal crops, and are responsible for causing severe yield losses (De Vallavieille-Pope *et al.,* 1995; Bravo *et al.,* 2003). Yellow rust caused by *Puccinia striiformis* is a foliar disease, which can reduce crop yields by up to 40%. Alternatively known as stripe rust, the pathogen produces yellow uredo spores on the leaves. Infection starts with chlorosis occurring parallel to leaf veins, in a narrow 2 mm wide stripe, which develops later into multiple yellow coloured rust pustules (De Vallavieille-Pope *et al.,* 1995). Disease presence can vary considerably between plants. In severe epidemics the yield can be reduced by up to 7 tonne ha^{-1} (Bravo *et al.,* 2003). Fusarium head blight is one of the most important pre-harvest diseases worldwide, reducing yield quantity and quality. The most aggressive and prevalent fusarium strain is *Fusarium graminearum,* which is a highly pathogenic strain producing mycotoxins, which can become a significant threat to both humans and animals. Fusarium head blight symptoms in wheat and barley appear in the head and peduncle tissues, causing discolouration and early senescence. Disease presence can vary considerably between plants (Desjardin, 2006; Brennan *et al.,* 2005; Leslie and Summerell, 2006; Rotter *et al.,* 1996), hence, it is required to adopt site specific treatments of fungal diseases.

Advanced methods for disease detection in crops are vital for improving the efficacy of treatment, reducing infection and minimising the losses to yield and quality. Traditionally, disease detection is carried out manually, which is costly, time consuming and requires relevant expertise (Schmale & Bergstrom, 2003; Bock *et al.,* 2010a). Alternative methods of detection are needed to enable mapping the spatial distribution of yellow rust and fusarium head blight. Among those methods, optical sensing methods are recommended candidates since they are non-destructive and allow for fast and repeated data acquisition throughout the growing season without inhibiting crop growth. It was recognised by West *et al.,* (2003) that although optical technologies are available for development into suitable disease

detection systems, many challenges are still needed to be overcome, and this is still arguably the case. Spectroscopy and imaging techniques have been used in disease and stress monitoring (Hahn, 2009). One of the optical methods reportedly used to measure disease in crops is hyperspectral imaging in the visible (vis) and/or the near infrared (NIR) spectral ranges. The reflectance at visible wavelength range is relevant to leaf pigmentation whilst the infrared wavelength range provides information on the physiological condition of the plant. The wavelength function for light intensity in hyperspectral imaging adds to the brightness information of the spectral image, providing a rapid image-contrast (Huang *et al.,* 2007). Within the visible spectrum, the radiation reflectance from an environmentally stressed plant will increase. This is due to an increase in the incidence reflection within the leaf of a stressed plant (Cibula and Carter, 1992). Bélanger *et al.,*(2008) showed that disease could be quantified on detached leaves, and reported that the ratio of blue (near 440 nm) over green (near 520 nm) intensities between the healthy and diseased tissue was significantly different shortly after inoculation. Using a vis-NIR imaging, Bravo *et al.,*(2003) detected early symptoms of yellow rust on winter wheat, with a quadratic discriminant model analysis, reporting a correct discrimination accuracy of 92–98%. To our knowledge none of the above studies incorporated the effect of water stress, in the prediction model of yellow rust and fusarium head blight intensity in cereal crops. Some studies have focused on bringing the technology to the field. However, the first step towards field application is to test the accuracy of the methods under laboratory conditions (allowing more control and observation of the crop), where disease and water stress are accounted for simultaneously.

The aim of this paper is to assess the potential implementation and performance of a hyperspectral imager for recognition of yellow rust and fusarium head blight diseases in winter wheat and winter barley under laboratory conditions, with the intention to establish calibration models and a spectral library for potential use under mobile on-line measurement conditions. Both diseases (yellow rust and fusarium head blight) and water stress were introduced and accounted for.

2 Materials and methods
2.1 Wheat and Barley cultivation and inoculation

Treated seeds of winter wheat *Triticum sativum* (Solstice variety) and winter barley *Hordeum vulgare* L. (Carat Variety) were grown outdoors in 600 x 400 mm trays (depth of 120 mm), with 100 seeds evenly sown and spaced in 5 parallel lines. After seeding the trays were predominantly rain fed, to reduce input of excess salts from treated tap water. Three treatments were adopted, where each treatment was triplicated in three separate trays. A total of 18 trays of wheat, and 18 trays of barley were grown for each of the following three treatments:

94   1) Treatment 1 – Healthy: consisting of six trays of each that were kept healthy by applying a broad

95   spectrum fungicide (Rubric and Epoxiconazole, at a rate of 1 l ha^{-1}).

96   2) Treatment 2 – Naturally (non-inoculated) yellow rust infected: consisting of six trays that were

97   not treated with fungicide, as these were to represent the more heavily infected yellow rust trays, and

98   were not inoculated with fusarium.

99   3) Treatment 3 – Fusarium inoculated: consisting of six trays of each that were infected with fusarium

100 as the crop first reached anthesis growing stage (Figure 1).

101 When the crop growth reached 'booting' growth stage 45 on the Zadoks scale (Zadoks et $al.,$ 1974),

102 half of trays in each treatment were water stressed using a transparent tarpaulin and water content was

103 monitored throughout the growing season using a moisture-probe ML3 Thetakit (Delta-T Devices Ltd,

104 Cambridge, UK). Yellow rust occurred naturally in the crops as early as growth stage 30. Therefore,

105 half of the crop trays were treated early with fungicide to fulfil treatments 2 and 3. This allowed for a

106 difference in intensity of yellow rust disease. Fusarium inoculation was applied to trays in treatment

107 3 at the anthesis crop growth stage. The spores were first cultivated in the laboratory by using the

108 following method. A 2% wheat agar was produced using 100 ml distilled water, with 2 g agar and 2 g

109 milled wheat. This was autoclaved at 120°C. Plates were poured to a consistent depth, and

110 inoculated with $Fusarium$ $graminearum$. The plates were grown for 5-7 days under UV light as this

111 was shown to help cause sporulation (Leach, 1967). The agar plates were subsequently agitated with

112 distilled water to suspend the spores with the concentration increased as necessary by gentle use

113 of the centrifuge. Spore concentrations were standardised at approximately 10^6 ml^{-1} using

114 serial dilutions and a haemocytometer. Every 1 m^2 of crop ear was inoculated with 100 ml of the

115 suspension, which is an adapted method from Lacey (1999). These trays were then kept under a high

116 humidity conditions for 24 hours.

2.2 Disease assessments

119 A common approach for disease assessments and general crop health is by visual inspection known as

120 diagnosis (Oberti et $al.,$ 2014). Chiarappa (1981) defined two distinct quantitative disease

121 measurements: 1) Disease incidence, which is the percentage of infected plants to the healthy and 2)

122 Disease severity, which is the amount of expressed disease tissue of a plant. These disease parameters

123 can be assessed objectively, with some potential risk of subjectivity. In the current work, we

124 considered the disease severity measured as % coverage. Each tray was assessed for both diseases at

125 four levels, namely, at the head (when present), at the flag leaves, 2nd and 3rd leaves (mid canopy), and

126 at the lower canopy, as explained next;

127 1) For fusarium infection, only the head of the crop was assessed, since fusarium head blight symptoms

128 in wheat and barley usually only appear in the head and peduncle tissues, causing discolouration and

129 early senescence. Earlier visual symptoms consist of a characteristic purple/pink discolouration. The

130 seed from fusarium head blight affected crop is often shrunken, with a bleached appearance (Andersen,

131 1948; Goswami and Kistler, 2004; McMullen *et al.,* 1997; Parry *et al.,* 1995). Impey (2012) confirmed

132 the presence of fusarium leaf lesions in Herefordshire, the leaf lesions are very unusual, and found

133 only in heavy infections.

134 The assessment of fusarium head blight considered both early and later symptoms. During the course

135 of the study the wheat and barley ears were categorized as healthy (0% infected), early infection, where

136 ears showed early symptoms with half the ears expressing late symptoms (around 50% infected), high

137 infection (around 75% infected) and full infection, where all the ears in the inoculated trays showed

138 late symptoms (around 100% infected).

139 2) For yellow rust infection, the three foliar levels were assessed for percent coverage of yellow rust

140 lesions. Infection starts with chlorosis occurring parallel to leaf veins, in a narrow 2 mm wide stripe,

141 developing into multiple yellow coloured rust pustules (De Vallavieille-Pope *et al.,* 1995). Average

142 disease coverage was given for all the plants in the assessment area at the three different stages. As

143 it's needed for each ground truth plot to have a singular assessment for the later analysis, the data from

144 each stage was combined and weighted appropriately according to HGCA (2008) recommendations;

145 that 80% of a wheat yield can be calculated from the top 3 leaves (Figure 2).

146

147 **2.3 Hyperspectral data capture**
148

149 A push broom hyperspectral imager (spectrograph) (HS spectral camera model from Gilden Photonics

150 Ltd., UK) was used to capture high-resolution (1,608 pixels) line images over 1 second, using a diode

151 array detector. It is a 12 bit Basler piA 1600-35 gm camera, with Schneider-Kreuznach XNP1.4/23 lens

152 and has a pixel pitch of 7.4 μm interpolated/averaged to 0.6 nm readings with a spectral range of 400 -

153 1000 nm. The reflected light from the target travels through the lens, past an entrance slit through a

154 series of inspector optics in the spectrograph and then split by the prism dispersing element into different

155 wavelengths. This sensor was chosen for its potential for being applied to crop canopy measurements,

156 and was of a lower price compared to comparable sensors, commercially available in the market.

The spectral data was captured at three separate places along the crop tray at slightly different positions. Captured in the form of a line array, each pixel has a spectrum and one detector per pixel across the swath. In order to compile a full image, every line across a target must be captured (Gilden Photonics Ltd, Glasgow, UK). When configured on a consistent moving platform, the imager sweeps across an area to build up an image. Due to practical constraints of applying a consistent moving platform, the spectraSENS v3.3 (Gilden Photonics Ltd, Glasgow, UK) software was adapted to record a single line array, which required an additional RGB photo taken by a 5 megapixel camera with a 3.85 mm f/2.8 lens at the same time of image capture, so that the scanned area could be comprehended. Two laser pointers were added at each side of the hyperspectral imager to indicate the area of the canopy to be scanned (Figure 3). The laser pointers were shut off when the spectral image was captured to remove any interference. The collected scans were corrected by means of a dark and a white reference (spectralon 99% white reflectance panel) providing the relative reflectance. The latter was used before spectral capture, and at 10 minute intervals until scanning was completed. The optimal configuration of the push broom hyperspectral imager including light sources was optimised in the laboratory (Whetton *et al.,* 2016). A schematic illustration of the configurations can be observed in Figure 3, where two 500 watt diffused broad spectrum halogen lamps were positioned at either end of the crop sample tray. Light angle was kept constant at 45°, which is suggested as the optimal angle to provide the strongest response (Huadong, 2001). The optimal configuration adopted included integration time, light height, light distance, camera height, and camera angle, of 50 ms, 1.2 m, 1.2 m, 0.3 m and 10°, respectively (Whetton *et al.,* 2016). These configurations were used in the current work, for crop canopy scanning that started at booting growth stage 60 on Zadok's scale and continued until reaching ripening at growth stage 87. Four scans collected at four growth stages are considered in this study for both wheat and barley: 1) at anthesis (GS 60), 2) at kernel development; early milk (GS 72), 3) at kernel development; late milk (GS 77), and 4) hard dough (GS 87) (Table 1).

2.4 Data pre-processing and modelling

If the spectral data are too noisy there is a risk that key features of the spectrum are hidden, which necessitates smoothing to remove noise. But, aggressive smoothing can also remove significant features (Dasu & Johnson, 2003), hence the need for a gentle smoothing to avoid losing of useful spectral features. Furthermore, a noisy spectrum can result in poor model performance, due to noise being considered a feature. Thus, the first step towards successful measurement should be to obtain a good quality spectrum. This was ensured in the current work by adopting the optimal configurations established in Whetton *et al.,* (2016). The three lines of captured spectral data from each tray at each

time were averaged first, before they were linked with the visual crop assessment. The spectral range outside of the 400 to 750 nm range was removed as it was noisy. The first and last 320 pixels from each line scan were removed due to variation and risk of overlapping the crop to the surrounding background. Both these pre-processing steps of the data are in line with Whetton *et al.,* (2016). The spectral data was averaged to reduce the number of wavelengths (variables), which was successively followed by maximum normalisation, Savitzky–Golay first derivative and smoothing (Mouazen *et al.,* 2006). Maximum normalisation is typically used to get all data to approximately the same scale, or to get a more even distribution of the variances and the average values. The maximum normalisation is a normalisation that "polarizes" the spectra. The peaks of all spectra with positive values scale to +1, while spectra with negative values scale to −1. Since all soil spectra in this study have positive values, the peaks of these spectra scaled to +1. This scaled spectra between 0 and +1. Using the Savitzky–Golay first derivative enables the computation of the first or higher-order derivatives, including a smoothing factor, which determines how many adjacent variables will be used to estimate the polynomial approximation used for derivatives. A second order polynomial approximation was selected. A 2:2 smoothing was carried out after the first derivative to decrease noise from the measured spectra. All pre-processing steps were carried out using Unscrambler 10 software (Camo Inc.; Oslo, Norway).

Analysis of variance (ANOVA) was used to analyse two spectral indices captured at growth stage 72. A factorial treatment structure was incorporated to test for differences between disease type (healthy, fusarium, yellow rust), water treatment (watered, water-stressed) and crop type (barley, wheat). In addition, a contrast was used to test for differences between healthy and diseased trays and between the different diseases. Analysis of the index SD was done on a log scale, whilst analysis of SQdiff was done on a sqrt scale to ensure homoscedascity of variance. GenStat 18th Edition (© VSN International Ltd, Hemel Hempstead, UK) was used to compute the ANOVA tables.

Principal component analysis (PCA) was used to investigate the multivariate hyperspectral response over the different scanning intervals for barley and wheat data separately. The first two principal components accounted for 92% of the variation in both the barley and wheat data. Consequently, for both crops, PCA provides a reasonable summary of the hyperspectral response in two dimensions.

Separate PLSR analyses were applied to each of the four scanning intervals to establish quantitative models to predict yellow rust and fusarium head blight infection (Table 1). This means that for each crop four PLSR analyses were carried out. Before PLSR analysis, data were divided into two sets of 80% (e.g., 43 samples) and 20% (e.g., 11 samples), representing the calibration and prediction

data sets (Tables 2 and 3), respectively. The pre-processed spectra and visual assessments of yellow rust and fusarium head blight of the calibration dataset were subjected to PLSR with leave-one-out full cross-validation to establish calibration models. The performance of these models was evaluated by predicting crop disease using the prediction dataset. Separate models for wheat and barley were developed and evaluated for yellow rust and fusarium head blight. The following models were developed and validated:

1) Yellow rust prediction in wheat and barley, estimated as % of disease symptoms spread on the leaves. This was referred to as yellow rust % coverage.

2) Fusarium head blight prediction in wheat and barley, estimated as % of infected ears. This was referred to as fusarium % coverage.

For both models, a logit transformation of the % coverage response was applied to ensure homoscedascity of variance. The inverse LOGIT function (exp(p)/(1+exp(p))) was applied before assessment of the prediction results. PLSR analysis was carried out using Unscrambler 10 software (Camo Inc.; Oslo, Norway). Outliers were detected, and removed to a maximum of 5% of the total input data. The model performance was evaluated in cross-validation and prediction by means of coeefecient of determination (R^2), root mean square error of prediction (RMSEP) and ratio of prediction deviation (RPD), which equals standard deviation divided by the RMSEP. In order to compare between the performances of the developed models we proposed classifying RPD values into the classes mentioned in Table 4. The entire pre-processed spectrum was used in both the PCA and PLSR analyses.

3 Results and discussion
3.1 Crop canopy spectra

Example of crop canopy spectra for wheat and barley are shown in Figure 4. The spectral signatures were selected to demonstrate clearly the variations in shape. An arrows have been added to highlight wavelengths that define spectrum regions containing the most visible variation between the two crops. In Figure 4, wheat has higher reflectance. This may be due to the particular spectrum selected, as generally the reflectance intensities of wheat and barley were witnessed to be similar. However, it may also be attributed to the larger leaf area of wheat, which reflected more light than barley, which has smaller surface area. Within the visible range of 400–550 nm, there is low reflectance due to larger

8

253 absorption of the light, attributed to the photosynthetic pigments of the plant leaves, governed by the

254 abundance of chlorophyll, which absorbs most of the light radiation (Gates *et al.,* 1965; Thomas &

255 Gausman, 1977). Both plant chlorophylls and carotenoids have strong absorption at 480 nm, the

256 waveband associated with blue colour (Hunt *et al.,* 2013). Another interesting band at 670 nm

257 (associated with red colour band at 680 nm) can be linked with chlorophyll a absorption that also

258 appears at 550 nm (Hunt *et al.,* 2013). The latter wavelength is designated as the green leaf reflectance

259 (Buscaglia and Varco, 2002 and Zhao *et al.,* 2005). The strongest absorption wavelength band appears

260 at the red edge around 715 nm, with deeper absorption in the barley spectrum than in wheat. Raper

261 and Varco (2015) found that the strongest wavelength correlations with leaf nitrogen concentration,

262 yield and plant total nitrogen content are near 700 nm. Further analysis of these bands as linked with

263 crop diseases studied is discussed below.

264 Average spectra of healthy, yellow rust and fusarium head blight infected wheat crop canopies at growth

265 stage 72 are plotted in Figure 5. While plots a, b and c juxtapose irrigated and water stressed spectra, plot

266 d compares between healthy and infected canopies under irrigated conditions. Generally, all spectra

267 are similar, although slight differences can be observed by close examination of individual plots

268 (Figure 5, b and c). The water-stressed spectra are less reflective than watered spectra, particularly

269 for yellow rust (Figure 5a). Slight differences in spectral shape can be observed in the healthy canopy

270 (a), which is in line with the findings from Earl and Davis (2003) who attributed these differences to

271 alterations in leaf internal structure, variations in leaf angle (due to wilting) and leaf area index. Lower

272 reflectance at the green edge (500-570 nm) and red edge (670-750 nm) can be attributed to water

273 stress. However, these slight differences may indicate that water-stress has only slight influence on crop

274 canopy, hence, on the performance of PLSR models in predicting yellow rust and fusarium head blight.

275 The influence of water stress on yellow rust infected crop canopy is more obvious, where the water-

276 stressed spectrum is consistently of lower reflectance (higher absorption) than the watered spectrum

277 throughout the entire waveband (Figure 5b). This indicates that water stress may have a considerable

278 influence on yellow rust prediction. However, spectra pre-processing e.g., maximum normalization used

279 in this study will eliminate difference in reflectance e.g., due to scattering, as all spectra will be scaled

280 between 0-1. Only a small deviation is observed between fusarium head blight infected spectra

281 (Figure 5c), indicating little effect of water stress on fusarium head blight prediction. This is supported

282 by the statistical analysis of the indices discussed below (Table 6).

283 A close examination of Figure 5d indicates notable differences in spectra between healthy, yellow rust

284 and fusarium head blight infected crop canopies under watered conditions. The healthy spectrum is of

285 lower reflectance than both infected spectra in the range between 400 to 700 nm. This could be

286 attributed to larger photosynthetic pigments of the plants associated with chlorophyll (Gates *et al.,*

287   1965; Thomas and Gausman, 1977). Cibula and Carter (1992) reported larger reflectance in infected

288   leaves than healthy leaves, which is in line with findings of the current study. Indeed, after crop

289   infection from foliar diseases, such as yellow rust, noteworthy visual symptoms can usually be

290   observed. Early symptoms such as chlorosis, associated with a reduction in chlorophyll results in

291   increasing reflectance due to a reduction in light absorption (Lorenzen and Jensen, 1989). Therefore,

292   the sharpest increase in reflectance from 650 to 700 nm takes place in the healthy spectrum. Figure 6

293   compares between the average spectra of healthy, yellow rust and fusarium head blight infected barley

294   canopy at growth stage 72. The water-stressed canopy spectrum shows more reflection or less

295   absorption than the watered canopy spectrum for the healthy canopy in Figure 6a. This may reflect

296   the darker (greener) canopy of the watered canopy resulting in larger absorption of light. This is in

297   line with findings of other researchers, who have attributed the increased reflectance of the healthy

298   canopy to early senescence caused by drought, and a reduction in chlorophyll absorption (Jamieson

299   *et al.,* 1995; Hunt *et al.,* 2013). With yellow rust infected canopy (Figure 6b), the opposite trend can

300   be observed, where higher reflectance is shown for the water-stressed canopy. This trend is observed

301   in both the wheat (Figure 5b) and barley (Figure 6b) canopies, indicating a larger influence of yellow

302   rust on crop canopy when combined with water stress, compared to fusarium (Figures 5c and 6c),

303   where the differences between watered and water-stressed are minimal. As for wheat canopy, yellow

304   rust infected canopy has again the highest reflectance, compared to those of fusarium head blight and

305   healthy canopies (Figure 6d). The % coverages of yellow rust and fusarium head blight is larger in

306   wheat than in barley. In wheat, yellow rust watered canopy have an average infection of 42%, yellow

307   rust water stressed 45%, fusarium watered 83%, fusarium water stressed 86%, whereas in barley,

308   these are 36%, 33%, 48% and 52%, respectively.

309   In order to quantify differences between healthy, yellow rust and fusarium head blight infected spectra

310   two indices were taken into account in this study, namely, standard deviation (SD) of all wavelengths in

311   the 500-650 nm range and squared difference (SQdiff) of 650 and 700 nm (Table 5). Moshou *et al.,*

312   (2004) recommended the use of wavelength range between 460 and 900 nm for successful yellow rust

313   detection. Bauriegel (2011) recommends spectral analysis using the range intervals of 500–533 nm

314   (green), 560–675 nm (yellow), 682–733 nm (red) and 927–931 nm (red edge) for recognition of

315   Fusarium head blight infection (in growth stages 71−85, according to zadoks scale). Krishna, *et al.,*

316   (2014), suggested particularly useful spectra wavelengths of 428, 672, and 1399, for quantitative

317   detection of yellow rust from healthy crop.

318   These two proposed indices show clear differences in response both in the different crops and the

319   different treatments. The largest differences are observed between infection type, a significant F statistic

of $F_{1,24}$=1199 (p<0.001) and $F_{1,24}$=33 (p<0.001) was observed for the comparison between fusarium infection and yellow rust infection, for index SD and SQdiff respectively.

Analysis of the index SD revealed significant differences in response in barley and wheat ($F_{1,24}$=94.59, p<0.001) and big differences between healthy and diseased trays ($F_{1,24}$=874.11, p<0.001). The largest differences were observed between fusarium infection and yellow rust infection ($F_{1,24}$=1199.23, p<0.001). In contrast, there was no evidence of a significant main effect of water stress ($F_{1,24}$= 1.79, p=0.193), meaning that on average (over all disease types and crops) there is no evidence of a difference in the SD index for watered and water stressed trays. However, analysis of the index SD does demonstrate a significantly different response to water stress both within different crops and under different disease infections (full ANOVA table is given in Table 6), i.e. the response to water stress is not the same in the different conditions.

Analysis of the index SQdiff revealed significant differences between healthy and diseased trays ($F_{1,24}$=12.66, p=0.002) and also significant differences between fusarium infection and yellow rust infection ($F_{1,24}$=33.29, p <0.001). Moreover, different responses in the different crops was observed ($F_{1,24}$=7.61, p=0.011) with a significant interaction between crop type and disease type indicating the index SQdiff responds differently to disease type in the different crops ($F_{1,24}$=9.88, p=0.004). There was no evidence to suggest a differing response to water treatment ($F_{1,24}$=0.07, p=0.799).

Although the largest SQdiff in reflectance between 650 and 700 nm is observed for the healthy canopy (both watered and water-stressed) of wheat, the smallest SD is observed for yellow rust (Table 5). For the barley canopy, the largest SD and SQdiff can be observed for fusarium head blight infected canopies, indicating that these proposed two indices respond differently for different crops (Table 5). Consequently, the two indices adopted in the current work highlight a distinguishable difference between the yellow rust, fusarium head blight and healthy wheat and barley crop canopies. It is important to mention that whilst these indices have worked in establishing a difference between yellow rust, fusarium and a healthy canopy at growth stage 72 in this paper, it may be specific to the method and equipment used. Further work should be undertaken to assess the reliability of such indices, if captured at different growth stages, under different circumstances, with alternative equipment. This is an important point to make as a strong correlation of time to spectral change was observed through PCA. The first two PCs (principal components) are shown in Figure 7 (for wheat) and figure 8 (for barley). The separation of observations in this two-dimensional representation is strongly associated with the time of scanning. Moreover, very little association with disease coverage could be discerned. This demonstrates that in the captured data when all timings are considered, the strongest influence on the canopies reflectance is time. These results supported the decision to split the scans per time of capture, for the PLSR of yellow rust and fusarium predictions.

3.2 Model performance for yellow rust detection

The PLSR cross-validation and prediction results for yellow rust detection in are shown in Table 7. Separate PLSR were carried out for each time intervals of T1, T3, T5 and T7 for barley and T2, T4, T6 and T8 for wheat (Table 1). The cross-validation results indicate good model performance for yellow rust % coverage in wheat and barley (R^2 values for wheat are 0.82, 0.92, 0.77 and 0.84, for T2, T4, T6 and T8 and barley 0.88, 0.78, 0.76 and 0.83 for T1, T3, T5 and T7, respectively), showing low root mean square errors of cross-validation (RMSECV) ranging from 3.3 to 8.8%. In general, the barley cross-validation results for yellow rust, have a slightly lower R^2 values and larger RMSECV than the corresponding values for wheat (Table 7). As yellow rust is a foliar disease, this reduction in prediction performance for barley may be attributed to the crop having a smaller flag leaf, and due to density of the crop, causing a smaller foliar area to be captured by the hyperspectral imager.

When the developed PLSR models where used to predict the yellow rust % coverage of 20% of samples (11 samples) in the prediction set, the RMSEP values in both wheat and barley show larger values in the predictions than in the cross-validations. However, RMSEP is a valuable index for assessing individual model performance, but is not recommended to compare the performance between different models (e.g., those for wheat and barley and between different growing stages), due to the different data range. To compare between the performances of different models, RPD was used in this work, according to the RPD classes proposed in the current work (Table 4). The RPD values for prediction of each timing (growth stage), shown in Table 7, suggest good prediction capability for 6 out of 8 growing stages (RPD ranges of 2.16-2.49 in wheat and 2.18-2.43 in barely), a very good prediction for T4 (kernel development, early milk (GS 72) in wheat (RPD = 2.79) and a moderate prediction capability for T5 (kernel development; late milk (GS 77) in Barely (RPD) = 1.83).

It is well known in spectral analysis that successful measurement of a concentration, be it soil properties or other, depends on presence of variability of that said concentration. For example, Kuang and Mouazen (2011) reported that although larger R^2 and RPD can be obtained with larger variability in soil analysis, larger RMSEP is to be expected. Furthermore, with a small variability, weak or even no correlation can be established with PLSR, so that no models can be developed. Having said that, we believe that the scale of variability in % coverage of yellow rust is rather small (Tables 2 & 3), although a reasonably high infection is recorded at few points (see the mean and SD values). The small variability may be due to the experiment being run in trays under rather controlled conditions, where only water is varied artificially. These controlled conditions may lead to small variability in yellow rust (Tables 2 & 3). The percentage of disease coverage which is a method discussed by Chiarappa

387 (1981) and defined as "disease severity", is the amount of expressed disease tissue of a plant. This

388 method can be objective, but is definitely not free of subjectivity. In the current study all

389 assessments are made by the same individual, which decreases the between assessment variability due

390 to the subjective nature of the measurement. The more spectral wavelength indices captured and

391 accounted for, the greater understanding of the object (Gilchrist, 2006). However, for noisy spectra

392 there is a need to minimise noise in the signal, by adopting an optimised measurement configuration

393 (Whetton *et al.,* 2016) and suitable spectra pre-processing. Furthermore, stresses in the field are

394 combined and might include water stress, nitrogen stress, disease stress, and other stresses that are

395 mainly reflected on crop canopy as a yellowing of the leaves. In the current work we have combined

396 water stress and yellow rust infection in the tray experiments, to evaluate the prediction accuracy

397 of the yellow rust models.

398 The results obtained in this study for yellow rust prediction encourage exploring the ultimate goal of

399 the current study, which is on-line measurement of yellow rust in the field using the hyperspectral

400 imager (400 – 750 nm). However, additional affecting parameters exist in the field on top of the water

401 stress accounted for in the current study, and these should also be evaluated. Using wheat trays under

402 glass house controlled conditions, Moshou *et al.* (2014) reported successful discrimination of water-

403 stressed from healthy plants with 99% accuracy. Their approach was based on a combination of

404 hyperspectral (460–900 nm) and fluorescence imagery and machine learning models. The early

405 success in field studies for hyperspectral imager's detection of yellow rust disease such as Moshou *et*

406 *al.* (2004) and Bravo *et al.* (2003) focused on the presence of yellow rust in the field, not necessarily

407 the intensity. Typically disease recognition attempts with hyperspectral and multispectral imaging are

408 targeted to leaves rather than the canopy (Bock *et al.,* 2010b). Whilst recent attempts using lower cost

409 solutions for disease quantification in wheat based on RGB images (Zhou *et al.,* 2015) provided larger

410 error margins. Compared to other studies the current work achieved moderate to very good accuracy

411 based only on a relatively cost-effective hyperspectral camera in the visible range only. In addition, we

412 have accounted for the effect of water stress in the experimental trial, hence, this effect was included

413 in the PLSR prediction models.

414

3.3 Model performance for fusarium head blight detection

416 The cross-validation results for % coverage of fusarium head blight indicate good model performance

417 in both wheat and barley (R^2 values for wheat are 0.84, 0.89, 0.81 and 0.83, for T2, T4, T6 and T8 and

418 barley 0.95, 0.83, 0.75 and 0.79 for T1, T3, T5 and T7, respectively), with RMSECV range of 8.6 to

419 29 % in wheat and 14 to 25 % in barley (Table 7). However these RMSECV ranges are higher than

420   those calculated for yellow rust. The lowest R^2 for cross-validation was once again for the late milk

421   stage. Due to the method of inoculation explained-above, there was little variability observed in fusarium

422   head blight disease intensity per timing (growing stage). Although the relatively low variability recorded

423   for fusarium, the cross-validation results for both wheat and barley indicate good model performances

424   (Table 7).

425   The prediction results indicate larger RMSEP values for fusarium head blight (RMSEP = 7.9 – 16.1 %

426   for wheat and 10.4 – 15.1 % for barley) are calculated than those for yellow rust (RMSEP = 7.2 – 8.8 %

427   for wheat and 7.2 – 8.1 for barley). However, for RPD, the opposite case is true. According to RPD values,

428   good (for one growing stage) to very good (for three growing stages) predictions are recorded for fusarium

429   in wheat, whereas very good predictions are calculated for the four growing stages in barley (Table 7).

430   Also, higher RPD values are calculated for the prediction of fusarium head blight in both crops. The lower

431   RMSEP values calculated for yellow rust than those for fusarium suggest higher prediction accuracy for

432   yellow rust (smaller error). This means that yellow rust can be detected with higher accuracy than

433   fusarium head blight, an observation to be taken into account for future variable rate applications or

434   relevant fungicides.

435   Fusarium head blight symptoms appear on crop heads at a late stage in the crop growing season

436   (normally only after anthesis, but potentially at head emergence), allowing for limited number of

437   scans to be collected. Bauriegel *et al.* (2011) claimed that *fusarium* head blight can be detected by

438   spectral analysis in the spectral range of 400–1000 nm, with an identification accuracy of 87%. These

439   authors advised that the ideal timing for measurement at the medium milk stage (growth stage 75),

440   though the scans were based on the crop ears against a black background. Delwiche *et al.* (2011)

441   successfully differentiated between healthy kernels from fusarium head blight infected,

442   reporting a 95% classification accuracy. The results reported in the current study support the previous

443   findings, as the highest prediction performance is recorded for the kernel development stages, at both

444   the early and late milk. Bauriegel *et al.* (2011) have also reported the highest measurement accuracy

445   of fusarium in the milk kernel development stage. However, the relatively lower RPD scores in the

446   earlier scans (T1 for barley and T2 for wheat), may be attributed to a smaller standard deviation of the

447   data sets (Tables 2 and 3).

448   In order to account for the temporal dependence in observations over the different scanning intervals

449   collected at the four growing stages in this study (Table 1), it was necessary to run a separate PLSR

450   analysis for each growing stage. This has resulted in a rather small number of samples for each PLSR

451   analysis (e.g., 43 and 11 for the calibration and prediction sets, respectively). Therefore, it is necessary

452   to consider a larger dataset in the PLSR analysis in a future work, and to explore new methods of data

analysis based on machine learning and/or image processing, or adopt a modelling approach that can explicitly account for temporal dependence/repeated measures structure. It is also suggested to adopt a data fusion approach of both spectra and images, which is expected to provide more reliable model prediction performance. However, the results reported in this work are successful and encouraging to suggest testing the proposed hyperspectral technique in the visible range of 400-750 nm, coupled with PLSR as a potential tool for on-line measurement of the named two fungal diseases. However, there are other affecting parameters in the field than water stress that should be accounted for, which include within field variability in soil properties, varying ambient light, sensor-to-crop canopy height and angle.

4 Conclusions

The study explored the potential of a hyperspectral line imager (400-750 nm) for the detection of yellow rust and fusarium head blight in wheat and barley, based on partial least squares regressing (PLSR) analysis. The experiment was carried out in the laboratory under partially controlled environmental conditions where water stress effect was introduced. The results reported allowed the following five main points to be concluded:

1) The standard deviation of the wavelength range from 500 to 650 nm and the squared difference between 650 nm and 700 nm are of interest in discrimination between healthy, from yellow rust or fusarium head blight infected wheat and barley canopy.

2) The principle component analysis run on canopy spectral data collected on healthy, yellow rust and fusarium infected crops at multiple growth stages, reveal temporal pattern and time serial autocorrelations, which suggested the need for separate PLSR for each growing stage.

3) The best PLSR prediction performance for yellow rust in wheat was at the early milk of the kernel development stage, whereas for barley the best performance was at the anthesis and the early milk stages.

4) The best PLSR prediction performance for fusarium was at both the early and late milk of the kernel development stages in both wheat and barley.

5) Although higher ratio of prediction deviations were calculated for fusarium head blight, the smaller root mean square error of prediction for yellow rust suggested more accurate measurement of the latter under laboratory conditions.

483   The laboratory trials in this study have been designed to emulate a field. The data used in the models

484   was all collected from the wheat and barley trays, designed to simulate a field canopy, so the variance

485   of reflectance due to canopy is included in the models. Whilst other properties such as illumination

486   angle, view positions, shadows, plant species, maturity and phenology can be controlled under

487   laboratory conditions, these parameters will have considerable influences under field conditions, which

488   need to be evaluated with a future work planned in Part 2 of this study.

489

Acknowledgement

495

References

497   Andersen AL. (1948). The development of Gibberella zeae head blight of wheat.
498   Phytopathology 38:595–611.

499   Bauriegel, E., Giebel, A., Geyer, M., Schmidt, U. and Herppich, W.B. (2011). Early detection of
500   Fusarium infection in wheat using hyper-spectral imaging.*Computers and Electronics in Agriculture,*
501*75*   (2), pp.304-312.

502   Bélanger M.C., Roger J.M., Cartolaro P., Viau A.A., Bellon-Maurel V., Detection of powdery mildew
503   in grapevine using remotely sensed UV-induced fluorescence, Int. J. Remote Sens., 29 (2008), pp. 1707–
504 172
505
506   Bock, C.H., Poole, G.H., Parker, P.E. and Gottwald, T.R. (2010a). Plant disease severity
507   estimated visually, by digital photography and image analysis, and by hyperspectral
508   imaging. *Critical Reviews in Plant Sciences,**29*(2), pp.59-107

509   Bock, C. H., Graham, J. H., Gottwald, T. R., Cook, A. Z., & Parker, P. E. (2010b). Wind speed effects
510   on the quantity of Xanthomonas citri subsp. citri dispersed downwind from canopies of grapefruit trees
511   infected with citrus canker. Plant Disease, 94(6), 725-736.

512   Bravo, C., Moshou, D., West, J., McCartney, A., & Ramon, H. (2003). Early disease detection in wheat
513   fields using spectral reflectance. Biosystems Engineering, 84(2), 137-145.

Brennan, J.M., Egan, D., Cooke, B.M, Doohan, F.M. (2005). Effect of temperature on head blight of wheat caused by Fusarium culmorum and F. graminearum. Plant Pathology 54, 156.

Buscaglia, H. J., & Varco, J. J. (2002). Early detection of cotton leaf nitrogen status using leaf reflectance. *Journal of Plant Nutrition, 25*, 2067–2080.

Chiarappa L., ed. (1981). Crop Loss Assessment Methods — Supplement 3. Wallingford; CAB Interationa Cibula WG, Carter GA. (1992). Identification of a far-red reflectance response to ectomycorrhizae in slash pine. *International Journal of Remote Sensing*, 13:925–32.

Dasu, T., & Johnson, T. (2003). Exploratory data mining and data cleaning (Vol. 479). John Wiley & Sons.

Delwiche, S.R., Kim, M.S. and Dong, Y. (2011). Fusarium damage assessment in wheat kernels by Vis/NIR hyperspectral imaging. *Sensing and instrumentation for food quality and safety*, 5(2):63 71.

Desjardin, A.E. (2006). Fusarium mycotoxins. Chemistry, Genetics, and Biology. APS Press, St. Paul, MN.
de Vallavieille-Pope, C., Huber, L., Leconte, M. and Goyeau, H. (1995). Comparative effects of temperature and interrupted wet periods on germination, penetration, and infection of Puccinia recondita f. sp. tritici and P. striiformis on wheat seedlings. *Phytopathology*, 85(4), pp.409-415.

Earl, H.J. and Davis, R.F. (2003). Effect of drought stress on leaf and whole canopy radiation use efficiency and yield of maize. *Agronomy journal*, 95(3), pp.688-696.

Fungicide Resistance Action Committee, (2010). FRAC Recommendations for Fungicide Mixtures Designed to Delay Resistance Evolution.

Gates, D.M., Keegan, H.J., Schleter, J.C. and Weidner, V.R. (1965). Spectral properties of plants. Applied optics, 4(1): 11-20.

Gilchrist J. R. (2006). Gilden Photonics Ltd and Timo Hyvärinen, Spectral Imaging Ltd. Hyperspectral Imaging Spectroscopy: A Look at Real-Life Applications. Photonics.com. [Online].

Godfray, H.C.J., Beddington, J.R., Crute, I.R., Haddad, L., Lawrence, D., Muir, J.F., Pretty, J., Robinson, S., Thomas, S.M. and Toulmin, C., (2010). Food security: the challenge of feeding 9 billion people. science, 327(5967), pp. 812-818.

Goswami RS, Kistler HC. (2004). Heading for disaster: Fusarium graminearum on cereal crops. Mol Plant Pathol 5:515–525

Hahn, F., (2009). Actual pathogen detection: Sensors and algorithms—a review. Algorithms 2, 301–338.

Hole, D., Perkins, A., Wilson, J. D., Alexander, I. H., Grice, P. V., & Evans, A. (2005). Does organic farming benefit biodiversity? Biological Conservation, 122, pp. 113–130.

Home Grown Cereal Authority (HGCA) (2008). The spring wheat disease management guide. Warwickshire: Home Grown Cereals Authority (HGCA Publication).

Huadong, G. (2001). Applications of Radar Remote Sensing in China. New York: Taylor and Francis inc. 56.

Huang, W., Lamb, D.W., Niu, Z., Zhang, Y., Liu, L. and Wang, J. (2007). Identification of yellow rust in wheat using in-situ spectral reflectance measurements and airborne hyperspectral imaging. *Precision Agriculture,8*(4-5), pp.187-197.

Hunt, E.R., Doraiswamy, P.C., McMurtrey, J.E., Daughtry, C.S., Perry, E.M. and Akhmedov, B., 2013. A visible band index for remote sensing leaf chlorophyll content at the canopy scale. *International Journal of Applied Earth Observation and Geoinformation, 21*, pp.103- 112

Impey, L. (2012). Fusarium found on wheat leaves in western England. Available: http://www.fwi.co.uk/articles/19/07/2012/134000/fusarium-found-on-wheat-leaves-in-western england.htm. Last accessed 14/10/2013

Jamieson, P.D., Martin, R.J., Francis, G.S. and Wilson, D.R., 1995. Drought effects on biomass production and radiation-use efficiency in barley. *Field Crops Research, 43*(2), pp.77-86.

Krishna, G., Sahoo, R.N., Pargal, S., Gupta, V.K., Sinha, P., Bhagat, S., Saharan, M.S., Singh, R. and Chattopadhyay, C. (2014). Assessing wheat yellow rust disease through hyperspectral remote sensing. *The International Archives of Photogrammetry, Remote Sensing and Spatial Information Sciences, 40*(8), p.1413.

Kuang, B.; Mouazen, A.M. (2011). Calibration of a visible and near infrared spectroscopy for soil analysis at field scales across three European farms. European Journal of Soil Science, 62(4): 629-636.

Lacey J, Bateman GL, Mirocha CJ. (1999). Effects of infection time and moisture on the development of ear blight and deoxynivalenol production by Fusarium species in wheat. Ann Appl Biol 134:277–283.

Leach, C. M. (1967). Interaction of near-ultraviolet light and temperature on sporulation of the fungi Alternaria, Cercosporella, Fusarium, Helminthosporium, and Stemphylium. Canadian Journal of Botany, 45(11), 1999-2016.

Leslie, J.F., Summerell, B.A. (2006). The Fusarium Laboratory Manual. Blackwell Publishing, Ames, IA

Lorenzen, B. and Jensen, A., (1989). Changes in leaf spectral properties induced in barley by cereal powdery mildew. *Remote Sensing of Environment, 27*(2), pp.201-209.

Maleki, M.R., Mouazen, A.M., Ramon, H. and De Baerdemaeker, J., (2007). Optimisation of soil VIS–NIR sensor-based variable rate application system of soil phosphorus. Soil and Tillage Research, 94(1), pp.239-250.

McMullen MP, Jones R, Gallenberg G (1997). Scab of wheat and barley: a re-emerging disease of devastating impact. Plant Dis 81:1340–1348

Moshou, D., Bravo, C.,West, J.,Wahlen, S., McCartney, A., Ramon, H. (2004). Automatic detection of 'yellow rust' in wheat using reflectance measurements and neural networks. Computers and Electronics in Agriculture 44 (3), 173–188.

Moshou, D., Pantazi, X.E., Kateris, D. and Gravalos, I. (2014). Water stress detection based on optical multisensor fusion with a least squares support vector machine classifier. *Biosystems Engineering, 117*, pp.15-22.

Mouazen, A., De Baerdemaeker, J. & Ramon, H. (2006). Effect of wavelength range on the measurement accuracy of some selected soil constituents using visual-near infrared spectroscopy. *Journal of Near Infrared Spectroscopy,* Volume 14, p. 189–199.

Oberti, R., Marchi, M., Tirelli, P., Calcante, A., Iriti, M., & Borghese, A. N. (2014). Automatic detection of powdery mildew on grapevine leaves by image analysis: Optimal view-angle range to increase the sensitivity. Computers and Electronics in Agriculture, 104, 1-8.

Parry DW, Jenkinson P, McLead L. (1995). Fusarium ear blight (scab) in small grain cereals- a review. Plant Pathol 44:207–238

Raper T. B. and Varco J. J. (2015) Canopy-scale wavelength and vegetative index sensitivities to cotton growth parameters and nitrogen status. Precision Agriculture, 16(1), pp 62–76)

Rotter, B.A., Prelusky, D.B., Pestka, J.J. (1996). Toxicology of deoxynivalenol (vomitoxin). Journal of Toxicology and Environmental Health 48, 1–34.

Schmale, D.G., III, & Bergstrom, G.C. (2003). Fusarium head blightin wheat. The Plant Health Instructor. http://dx.doi.org/10.1094/PHI-I-2003-0612-01.

Thomas, J.R. and Gausman, H.W. (1977). Leaf reflectance vs. leaf chlorophyll and carotenoid concentrations for eight crops. *Agronomy journal,69*(5), pp.799-802

West, J.S., Bravo, C., Oberti, R., Lemaire, D., Moshou, D. and McCartney, H.A. (2003). The potential of optical canopy measurement for targested control of field crop diseases. *Annu. Rev. Phytopathol, 41*, pp.593-614.

Whetton, R.L., Waine, T.W. and Mouazen, A.M. (2017). Optimising configuration of a hyperspectral imager for on-line field measurement of wheat canopy. Biosystems engineering, *155,* pp.84-95.

Wittry, D.J. and Mallarino, A.P., (2004). Comparison of uniform-and variable-rate phosphorus fertilization for corn–soybean rotations. Agronomy Journal, 96(1), pp.26-33.

Zadoks, J.C.; T.T. Chang, C.F. Konzak (1974). "A decimal code for the growth stages of cereals. Weed Research 14 (6): 415–421. doi:10.1111/j.1365-3180.1974.tb01084.x.

Zhao, D., Reddy, K. R., Kakani, V. G., Read, J. J., & Koti, S. (2005). Selection of optimum reflectance ratios for estimating leaf nitrogen and chlorophyll concentrations of field-grown cotton. *Agronomy Journal, 97*, pp. 89–98.

Zhou, B., Elazab, A., Bort, J., Vergara, O., Serret, M.D. and Araus, J.L. (2015). Low-cost assessment of wheat resistance to yellow rust through conventional RGB images. *Computers and Electronics in Agriculture, 116*, pp.20-29.

Figure captions

Figure 1: Fusarium inoculation of wheat and barley trays in the laboratory. Inoculation took place at the anthesis crop growth stage.

Figure 2: Illustrating influence of foliar health on yield (HGCA, 2008). The weight given in this study was as follows; flag leaf 55%, mid canopy 40%, and lower canopy 5%. This allowed a single yellow rust assessment to be associated to a tray.

Figure 3: Schematic illustration of the laboratory configurations of hyperspectral camera and light source (Whetton *et al.,* 2016).

Figure 4: Example spectra of wheat and barley canopy, after white and dark corrections.

Figure 5: Comparison of an average wheat crop canopy (growth stage 72) spectra between watered (-) and water-stressed (----) treatments for healthy (a), yellow rust infected (b) and fusarium infected (c) crop canopy. Panel d compares canopy spectra under watered conditions of healthy (---), yellow rust (---) and fusarium (-).Watered yellow rust had an averaged infection of 42%, water stressed yellow 45%, watered fusarium 83%, and water stressed fusarium 86%.

Figure 6: Comparison of an average barley crop canopy (growth stage 72) spectra between watered (-) and water-stressed (----) treatments for a) healthy , b) yellow rust infected and c) fusarium infected crop canopy. Panel d compares canopy spectra under watered conditions of healthy (---), yellow rust (---) and fusarium (-). Watered yellow rust had an average infection of 36%, water stressed yellow rust 33%, watered fusarium 48%, and water stressed fusarium 52%.

Figure 7: Principal component analysis (PCA) similarity map of wheat canopy spectral data determined by principal components 1 (PC1) and 2 (PC2), showing separation of different spectra collected at Timing 2 (T2) of anthesis growth stage 60, T4 of early milk growth stage 72, T6 of late milk growth stage 77, and T8 of hard dough growth sage 87.

Figure 8: Principal component analysis (PCA) similarity map of barley canopy spectral data determined by principal components 1 (PC1) and 2 (PC2), showing separation of different spectra

657   collected at Timing 1 (T1) of anthesis growth stage 60, T3 of early milk growth stage 72, T5 of late

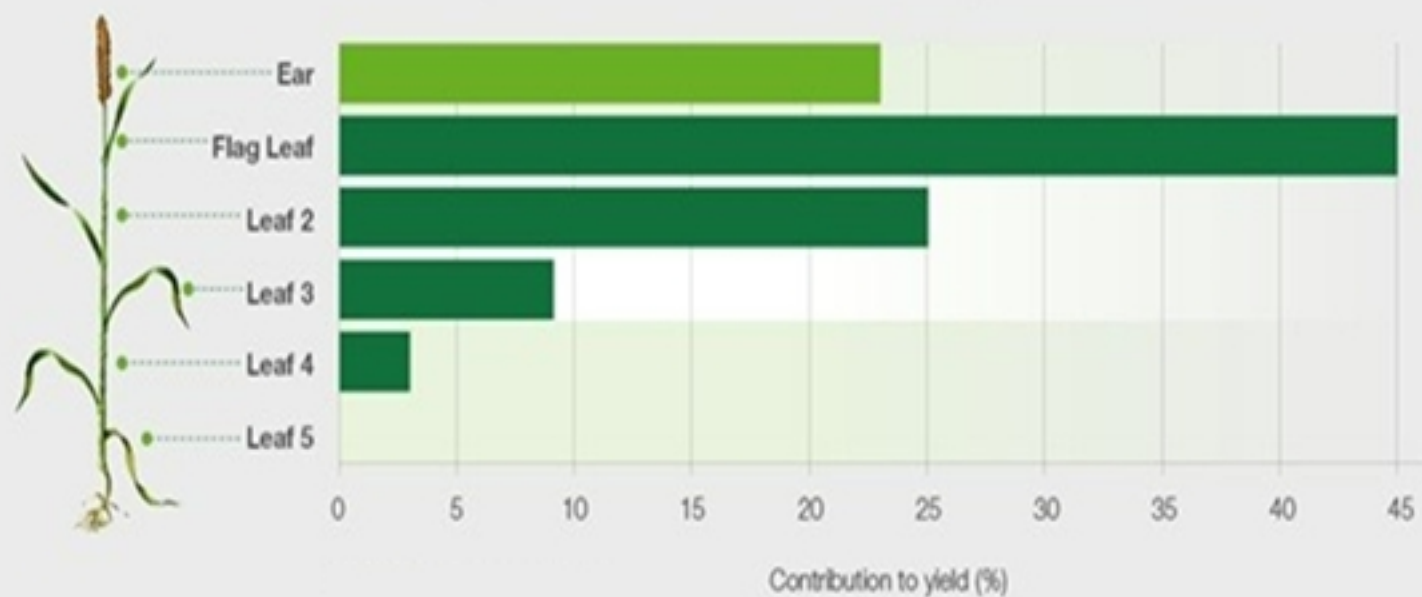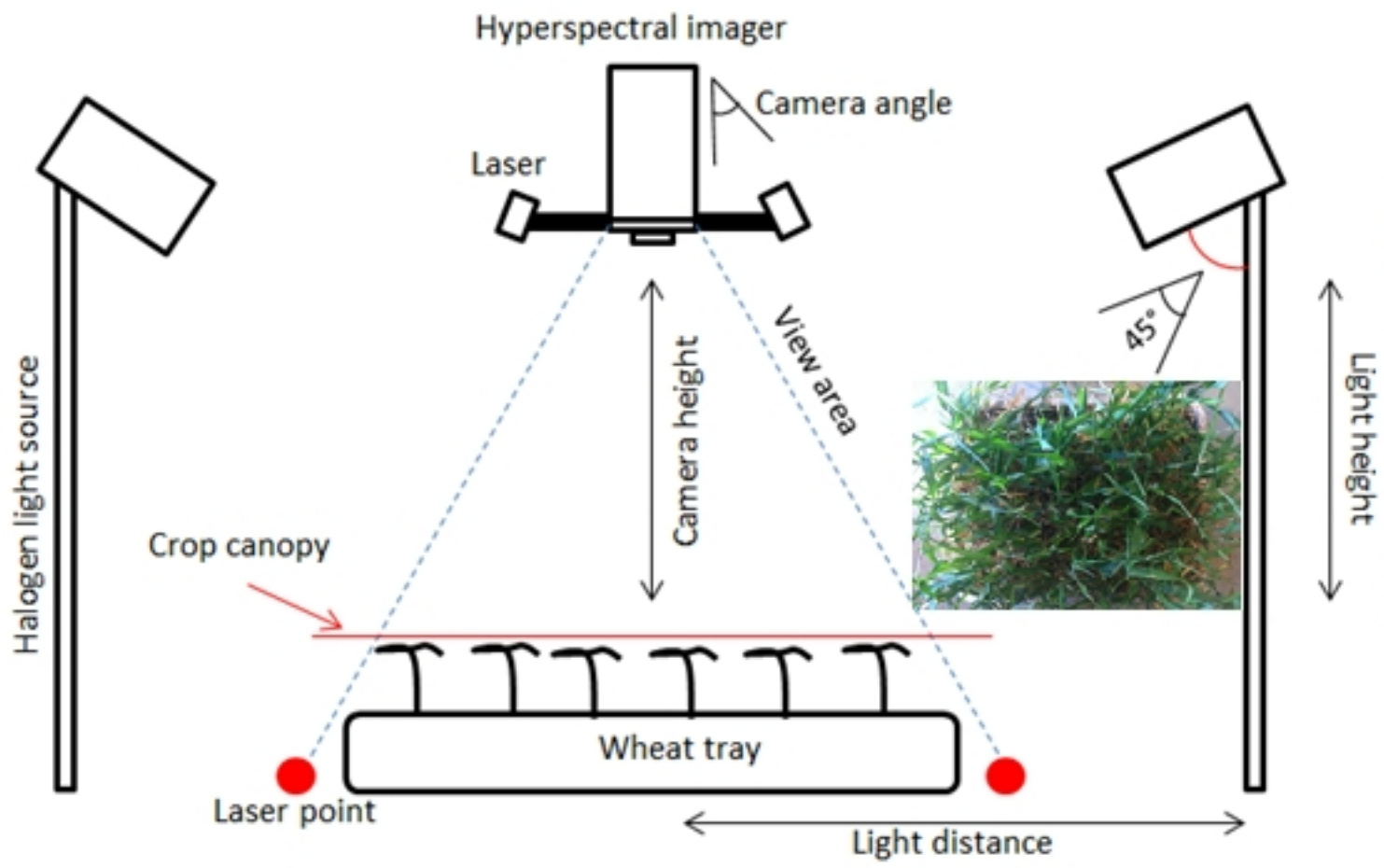658   milk growth stage 77, and T7 of hard dough growth sage 87.
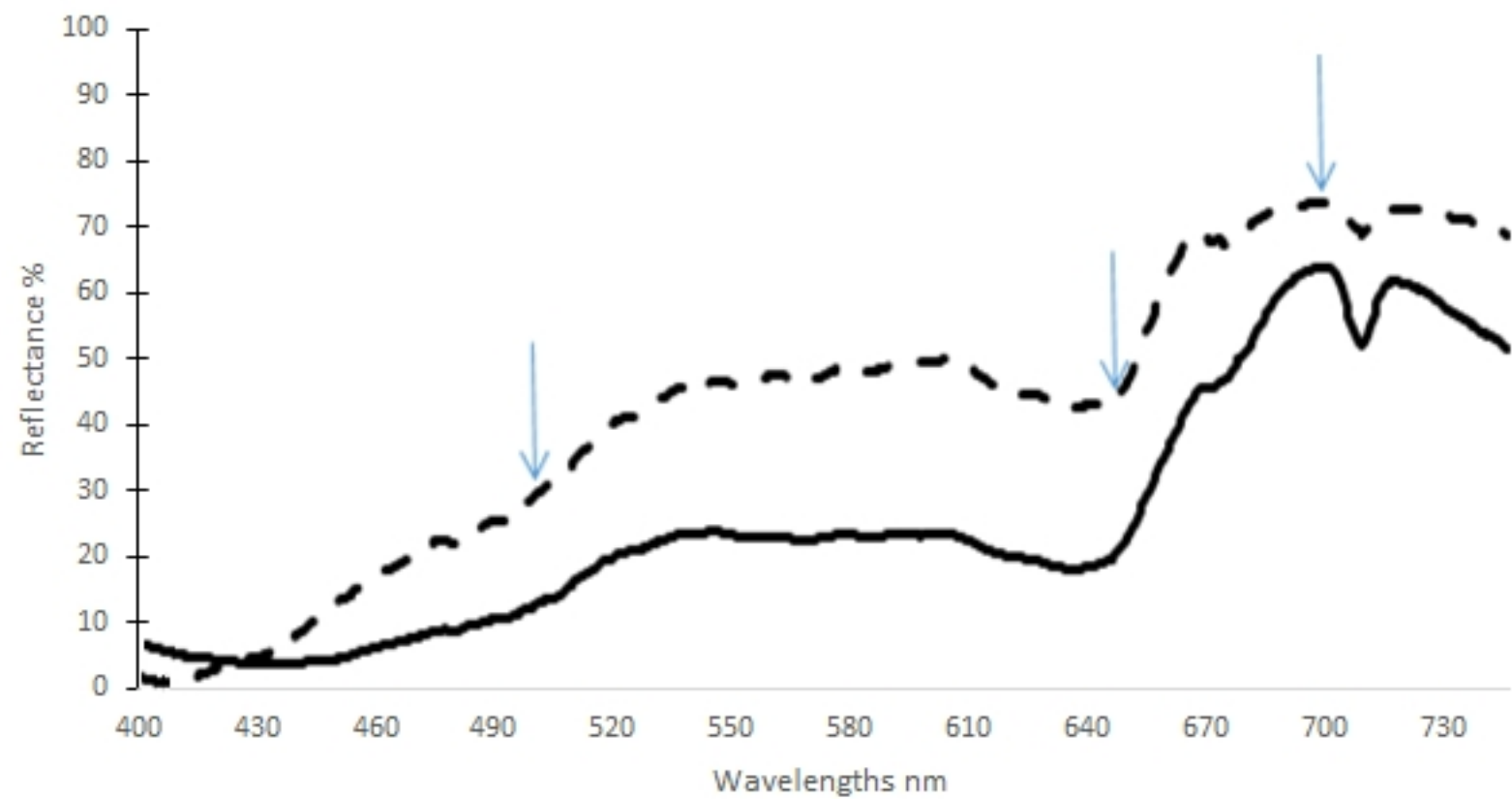
Fusarium suspension
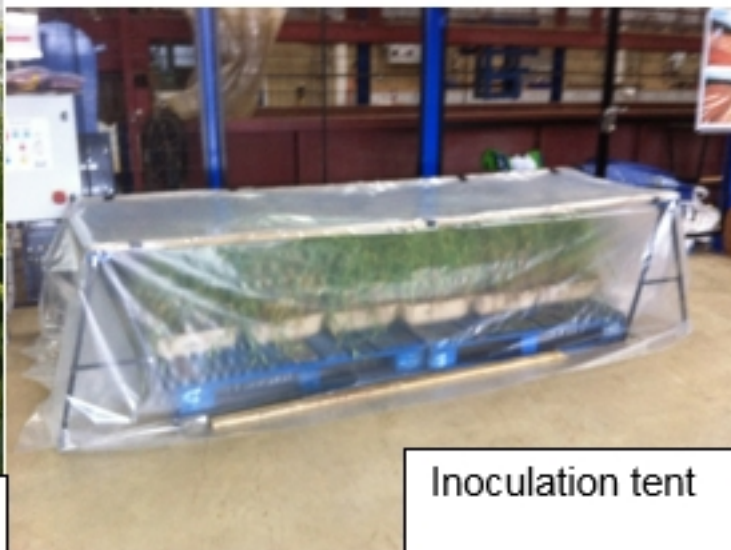
Inoculation tent

80% of wheat yield comes from the top three leaves

a)

b)

c)

d)
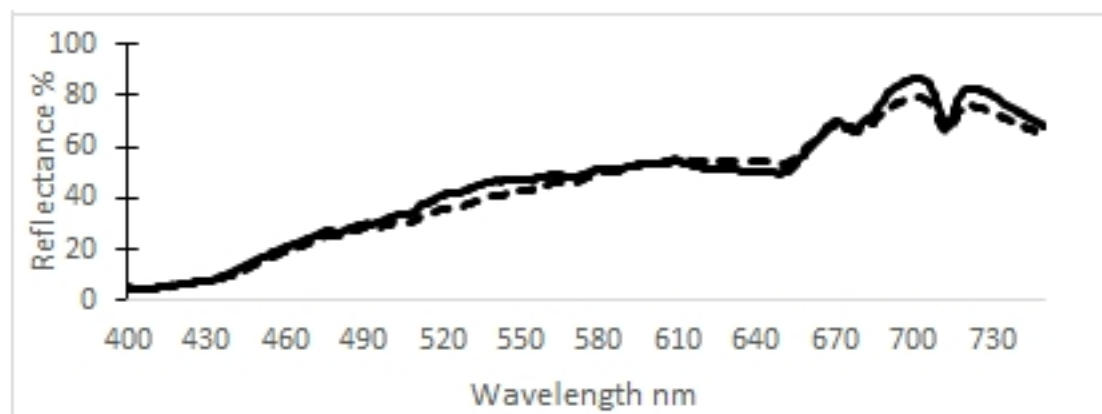
a)
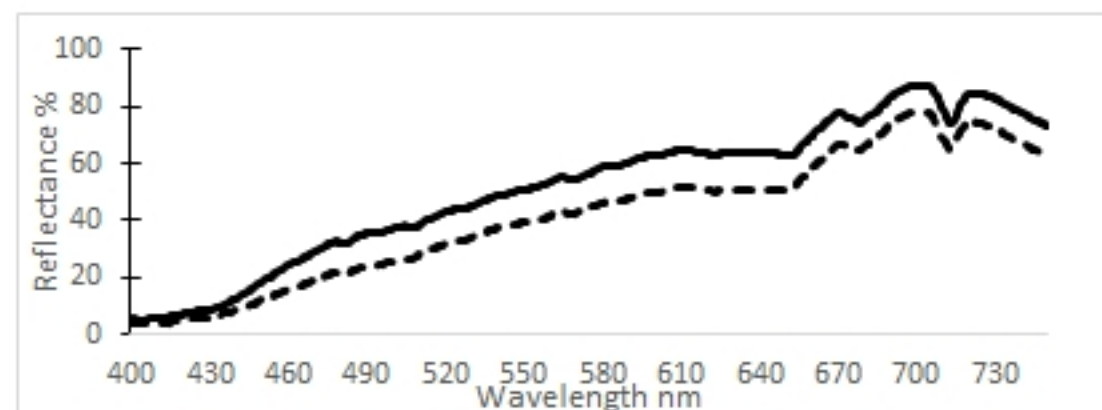
b)

c)
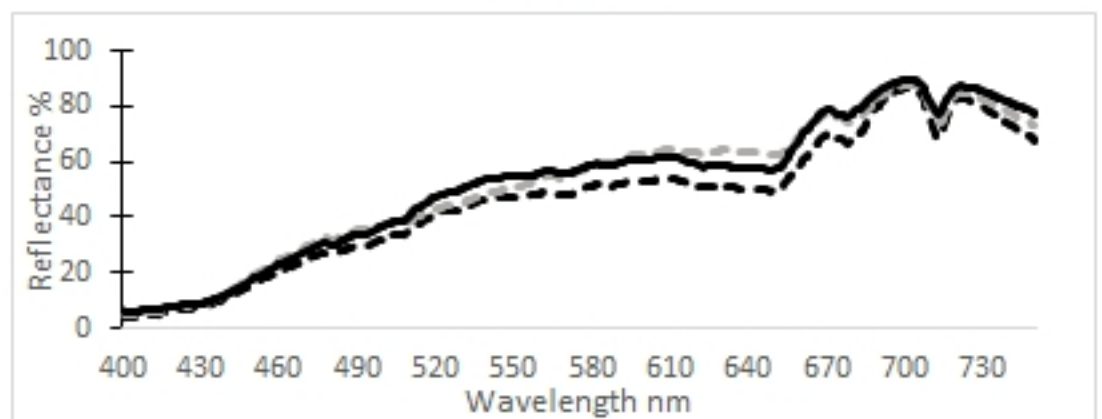
d)

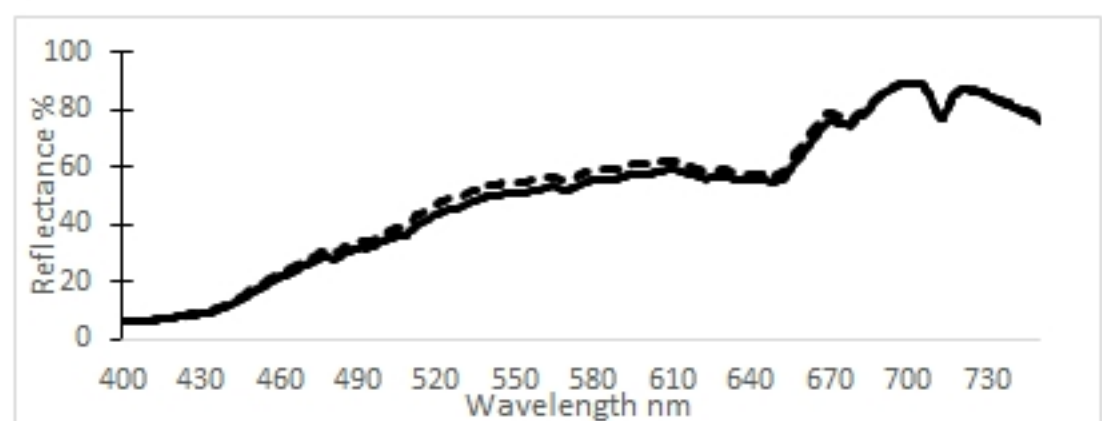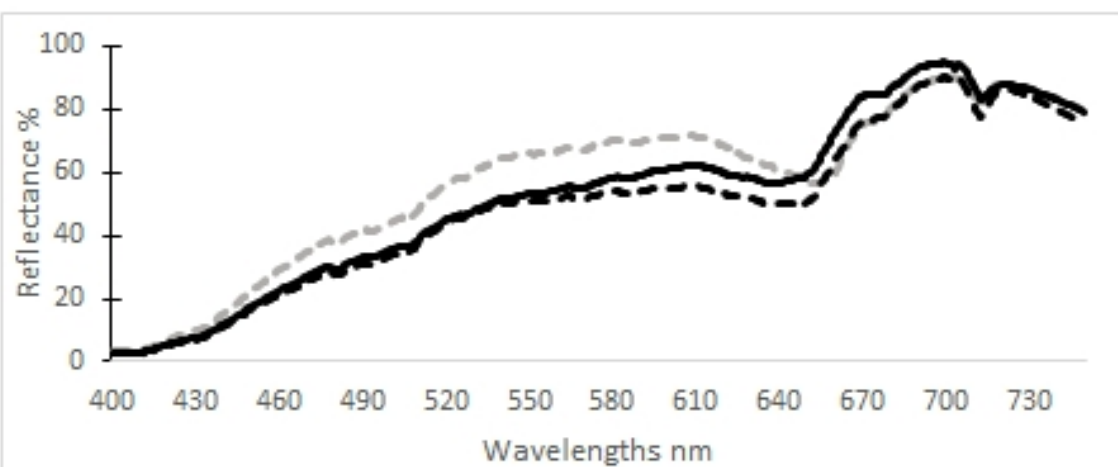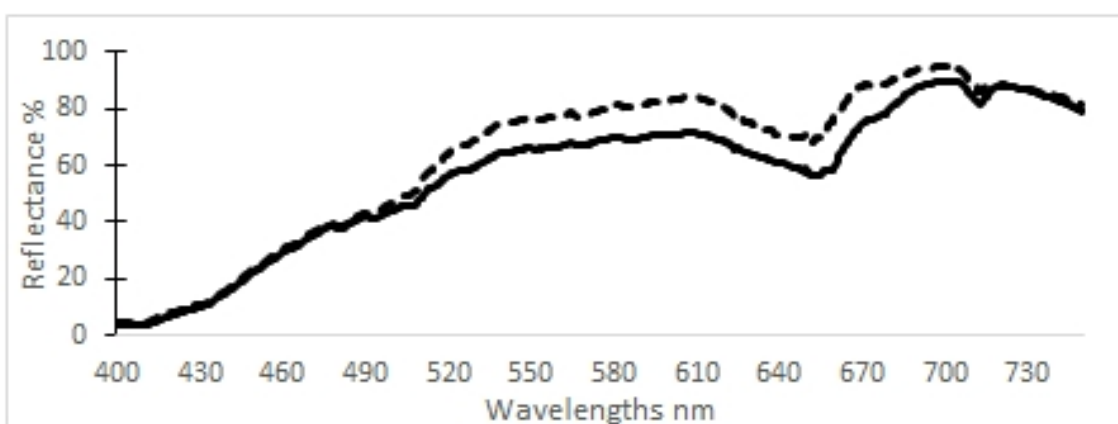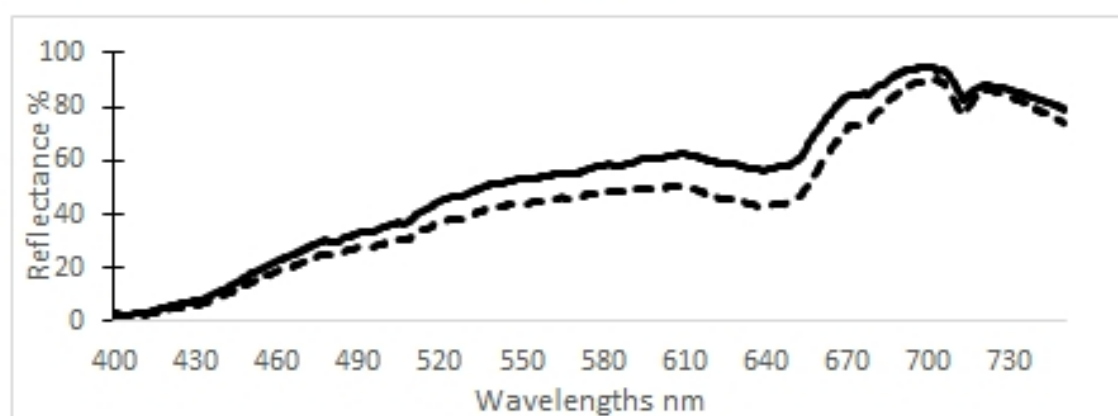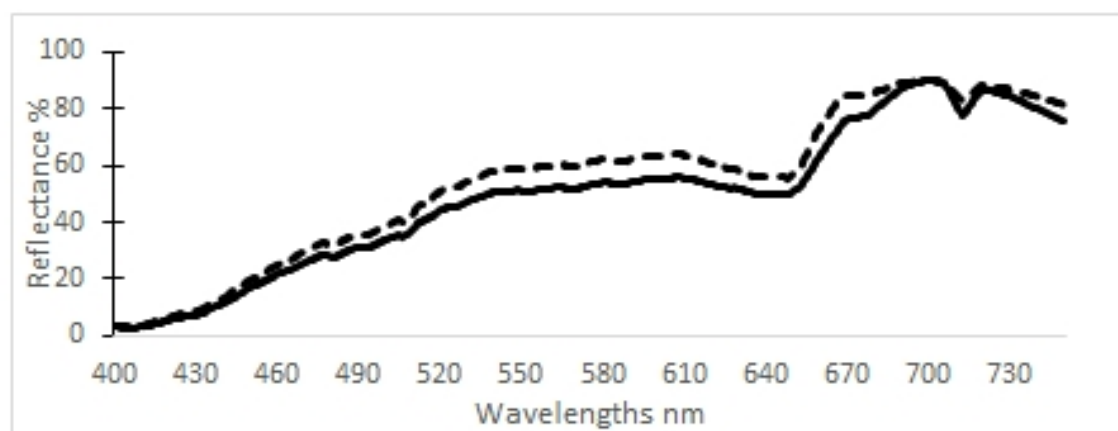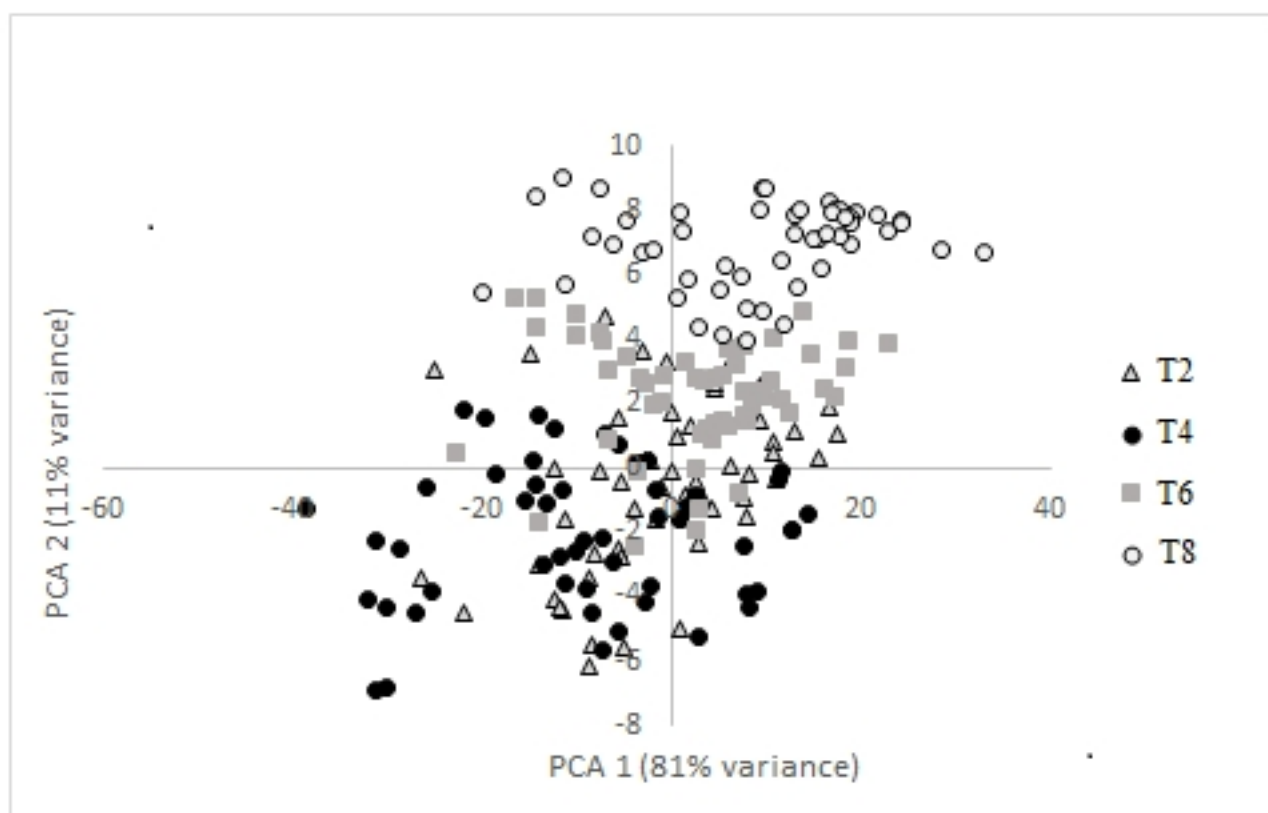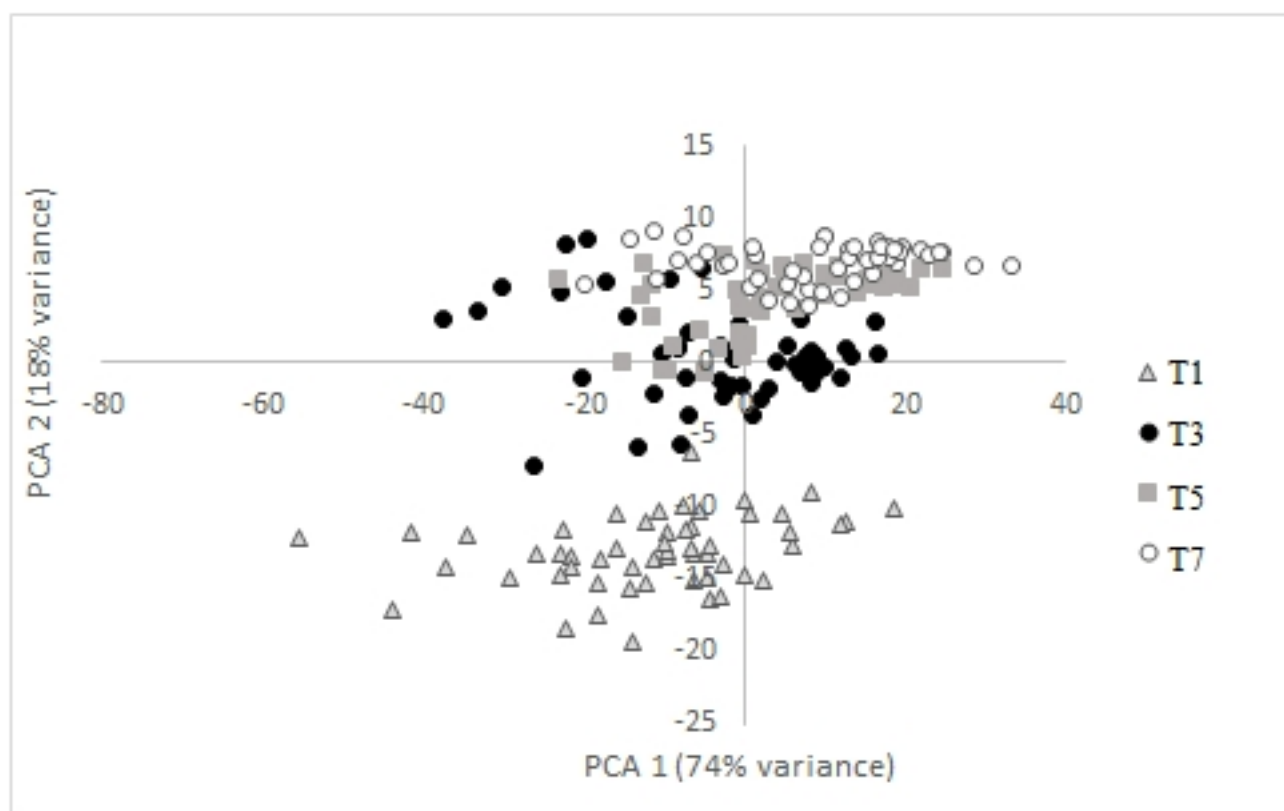**Table 1:** Hyperspectral scanning intervals of the wheat and barley trays, at four growth stages (GS) according to Zadoks scale (Zadoks *et al.,* 1974).

	Timing	Growth stage
Barley	1 (T1)	Anthesis (GS 60)
	3 (T3)	Kernel development; early milk (GS 72)
	5 (T5)	Kernel development; late milk (GS 77)
	7 (T7)	Hard dough (GS 87)
Wheat	2 (T2)	Anthesis (GS 60)
	4 (T4)	Kernel development; early milk (GS 72)
	6 (T6)	Kernel development; late milk (GS 77)
	8 (T8)	Hard dough (GS 87)

Table 2: Statistics of % coverage of both fungal diseases of wheat samples used in the partial least squares regression (PLSR) analyses, with 80% and 20% of samples were considered for cross-validation and prediction, respectively, at four separate timings (growth stages).

	Yellow rust				Fusarium			
	T2	T4	T6	T8	T2	T4	T6	T8
Cross-validation								
Sample Nr.	43	43	43	43	43	43	43	43
Maximum (%)	70	65	55	40	55	100	100	100
Minimum (%)	0	0	0	0	0	0	0	0
Mean (%)	30.4	20.8	17.4	15.9	17.5	24.1	30.1	31.5
SD (%)	21.4	11.8	11	11.3	23.0	32.4	43.2	45.0
Prediction								
Sample Nr.	11	11	11	11	11	11	11	11
Maximum (%)	70	70	50	60	50	100	100	100
Minimum (%)	0	10	5	0	0	0	0	0
Mean (%)	33.6	30	19.4	17.9	12	40	47	34
SD (%)	20.1	26.1	19	16.3	20.4	47.6	49.7	44.5

SD is standard deviation; T2 is anthesis growth stage 60; T4 is early milk growth stage 72; T6 is late milk growth stage 77; and T8 of hard dough growth sage 87 in wheat.

Table 3: Statistics of % coverage of both fungal diseases in barley samples used in the partial least squares regression (PLSR) models, with 80% and 20% of samples were considered for cross validation and prediction, respectively, at four separate timings (growth stages).

	Yellow rust				Fusarium			
	T1	T3	T5	T7	T1	T3	T5	T7
Cross validation								
Sample Nr.	43	43	43	43	43	43	43	43
Maximum (%)	50	60	60	55	50	75	100	100
Minimum (0)	0	0	0	0	0	0	0	0
Mean (%)	15.6	14.3	13.2	9.5	16	22.3	26.8	29.2
SD (%)	9.5	10.7	13.3	13.5	22.1	31.6	39.2	41.2
Prediction								
Sample Nr.	11	11	11	11	11	11	11	11
Maximum (%)	60	60	45	55	50	75	100	95
Minimum (%)	0	5	5	2	0	0	0	0
Mean (%)	17.7	18	17.3	14.3	16	17	31	24
SD (%)	18.8	15.4	14.2	16.4	22.1	30.4	45.5	37.1

SD is standard deviation; T1 is anthesis growth stage 60; T3 is early milk growth stage 72; T5 is late milk growth stage 77; T7 is hard dough growth sage 87 in barely.

Table 4: Classes of the ratio of prediction deviation (RPD) and their suitability for predicting yellow rust and fusarium head blight in cereal crops, and is based on the classifications..

RPD range	Class and prediction capability	Prediction Category
< 1	Poor model predictions - not useful.	A
1-1.5	Possibility to discriminate between low and high values	B
1.5-2.0	Moderate prediction capability	C
2.0-2.5	Good prediction capability	D
2.5-3.0	Very good prediction capability	E
>3.0	Excellent prediction capability	F

Table 5: Spectral differences indicated as standard deviation (SD) of the 500-650 nm range and squared difference (SQdiff) of 650 and 700 nm, calculated on the maximum normalised spectra for healthy, yellow rust, and fusarium infected wheat and barley canopies under watered and water-stressed conditions.

	SD 500-650 (nm)	Squared difference of 650 & 700 (nm)
Wheat		
Yellow rust watered	0.089	0.062
Yellow rust water-stressed	0.081	0.076
Healthy watered	0.057	0.15
Healthy water-stressed	0.063	0.14
Fusarium watered	0.16	0.10
Fusarium water-stressed	0.15	0.11
Barley		
Yellow rust watered	0.056	0.08
Yellow rust water-stressed	0.061	0.077
Healthy watered	0.051	0.15
Healthy water-stressed	0.065	0.18
Fusarium watered	0.15	0.25
Fusarium water-stressed	0.13	0.18

Table 6: Analysis of Variance (ANOVA) tables for the analysis of transformed spectral indices over the different treatments. Analysis of the index the squared difference of 650 and 700 nm (sqDiff) was done on the square root scale, whilst analysis of the index standard deviation (SD) is done on of the range 500-650 nm.

log(SD)

	d.f.	s.s.	m.s.	v.r.	F pr.
Disease Status (Healthy vs Infected)	1	7.48442	7.48442	874.11	<.001
Water (Watered vs Water stressed)	1	0.015325	0.015325	1.79	0.193
Crop (Barley vs Wheat)	1	0.809884	0.809884	94.59	<.001
Disease Status: Disease Class (Fusarium vs Yellow rust)	1	10.26827	10.26827	1199.23	<.001
Disease Status:Water	1	0.273841	0.273841	31.98	<.001
Disease Status:Crop	1	0.233846	0.233846	27.31	<.001
Water:Crop	1	0.053444	0.053444	6.24	0.02
Disease Status:Disease Class:Water	1	0.054515	0.054515	6.37	0.019
Disease Status:Disease Class:Crop	1	0.323653	0.323653	37.8	<.001
Disease Status:Water:Crop	1	0.001909	0.001909	0.22	0.641
Disease Status:Disease Class:Water:Crop	1	0.051774	0.051774	6.05	0.022
Residual	24	0.205497	0.008562	1.05	

sqrt(SQdiff)

	d.f.	s.s.	m.s.	v.r.	F pr.
Disease Status (Healthy vs Infected)	1	0.118056	0.118056	12.66	0.002
Water (Watered vs Water stressed)	1	0.000618	0.000618	0.07	0.799
Crop (Barley vs Wheat)	1	0.07096	0.07096	7.61	0.011
Disease Status:Disease Class (Fusarium vs Yellow rust)	1	0.310476	0.310476	33.29	<.001
Disease Status:Water	1	0.000456	0.000456	0.05	0.827
Disease Status:Crop	1	0.013211	0.013211	1.42	0.246
Water:Crop	1	0.001336	0.001336	0.14	0.708
Disease Status:Disease Class:Water	1	0.015536	0.015536	1.67	0.209
Disease Status:Disease Class:Crop	1	0.092105	0.092105	9.88	0.004
Disease Status:Water:Crop	1	0.012195	0.012195	1.31	0.264
Disease Status:Disease Class:Water:Crop	1	0.012502	0.012502	1.34	0.258
Residual	24	0.22381	0.009325	5.08	

Table 7: Summary of model prediction performance for yellow rust and fusarium head blight % coverage in wheat and barley in cross-validation and prediction. Results are shown for the determination coefficients (R^2), root mean square error of the prediction (RMSEP) and cross validation (RMSECV), and the ratio of prediction deviation (RPD), which is the standard deviation divided by RMSEP

			Cross-validation		Prediction			
			RMSECV (%)	R^2	RMSEP (%)	R^2	RPD	PCat
Wheat	*fusarium*	Timing 2	8.6	0.84	7.9	0.84	2.45	D
		Timing 4	27.7	0.89	15.1	0.91	2.97	E
		Timing 6	22.0	0.81	16.1	0.91	2.92	E
		Timing 8	29.0	0.83	16.0	0.93	2.83	E
	yellow rust	Timing 2	6.2	0.82	7.7	0.86	2.49	D
		Timing 4	5.0	0.92	8.8	0.91	2.79	E
		Timing 6	3.3	0.77	8.3	0.91	2.17	D
		Timing 8	7.0	0.84	7.2	0.86	2.16	D
Barley	*Fusarium*	Timing 1	14.9	0.95	14.4	0.97	2.52	E
		Timing 3	14.0	0.83	10.4	0.86	2.69	E
		Timing 5	14.0	0.75	15.5	0.93	2.72	E
		Timing 7	25.0	0.79	15.1	0.88	2.62	E
	yellow rust	Timing 1	8.8	0.88	8.1	0.90	2.43	D
		Timing 3	4.8	0.78	5.8	0.92	2.41	D
		Timing 5	3.9	0.76	7.6	0.71	1.83	C
		Timing 7	4.4	0.83	7.2	0.86	2.18	D

PC at timings in prediction category, to those detailed in Table 4.

Hyperspectral measurements of yellow rust and fusarium head blight in cereal crops: Part 1: Laboratory study

Whetton, Rebecca L.